

See discussions, stats, and author profiles for this publication at: <https://www.researchgate.net/publication/263990588>

# Best of Both Worlds: Conjugated Polymers Exhibiting Good Photovoltaic Behavior and High Tensile Elasticity

ARTICLE *in* MACROMOLECULES · MARCH 2014

Impact Factor: 5.8 · DOI: 10.1021/ma500286d

---

CITATIONS

22

---

READS

18

## 4 AUTHORS, INCLUDING:



Adam D. Printz

University of California, San Diego

18 PUBLICATIONS 119 CITATIONS

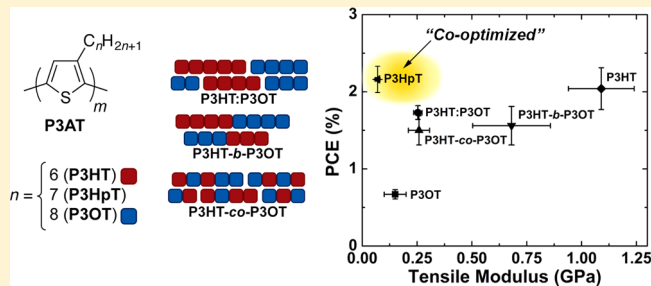
SEE PROFILE

## Best of Both Worlds: Conjugated Polymers Exhibiting Good Photovoltaic Behavior and High Tensile Elasticity

Suchol Savagatrup,<sup>†</sup> Adam D. Printz,<sup>†</sup> Daniel Rodriguez, and Darren J. Lipomi\*

Department of NanoEngineering, University of California, San Diego, 9500 Gilman Drive, Mail Code 0448, La Jolla, California 92093-0448, United States

**ABSTRACT:** This paper examines a series of poly(3-alkylthiophene)s (P3ATs), a class of materials for which mechanical compliance and electronic performance have been observed to be in competition. P3ATs with longer alkyl side chains ( $n \geq 8$ ) have high elasticity and ductility, but poor electronic performance (as manifested in photovoltaic efficiency in blends with fullerenes); P3ATs with shorter chains ( $n \leq 6$ ) exhibit the opposite characteristics. A series of four polymer films in which the average length of the side chain is  $n = 7$  is tested using mechanical, spectroscopic, microscopic, and photovoltaic device-based measurements to determine whether or not it is possible, in principle, to maximize both mechanical and electronic performance in a single organic semiconductor (the “best of both worlds”). The four polymer samples are (1) a physical blend of equal parts P3HT and P3OT (P3HT:P3OT,  $n = 6$  and  $n = 8$ ), (2) a block copolymer (P3HT-*b*-P3OT), (3) a random copolymer (P3HT-*co*-P3OT), and (4) poly(3-heptylthiophene) (P3HpT,  $n = 7$ ). The tensile moduli obtained by mechanical buckling correlate well with spectroscopic evidence (using the weakly interacting H aggregate model) of a well-ordered microstructure of the polymers. The block copolymer was the stiffest of the hybrid samples (680  $\pm$  180 MPa), while P3HpT exhibited maximum compliance (70  $\pm$  10 MPa) and power conversion efficiency in a 1:1 blend with the fullerene PC<sub>61</sub>BM using stretchable electrodes (PCE = 2.16  $\pm$  0.17%) that was similar to that of P3HT:PC<sub>61</sub>BM. These analyses may permit the design of organic semiconductors with improved mechanical and electronic properties for mechanically robust and stretchable applications.



### 1. INTRODUCTION AND BACKGROUND

There is an apparent competition between electronic performance and mechanical compliance in semiconducting polymers.<sup>1–4</sup> We previously observed an increase in elasticity in a series of regioregular poly(3-alkylthiophene)s (P3ATs) with increasing side-chain length (from  $n = 4$  to 12, Figures 1 and

attributed to the rigid,  $\pi$ -conjugated main chains and the three-dimensionally ordered crystallites generally regarded as beneficial for charge transport.<sup>1–4</sup> Crystallinity, however, is correlated with high stiffness and low ductility of the highest-performing pure polymers and—for organic solar cells (OSCs)—polymer:fullerene composites.<sup>1–4</sup>

The competing attributes of compliance and performance have significant consequences for the environmental stability of ultrathin OSCs<sup>9</sup> and devices based on organic thin-film transistors (OTFTs).<sup>10</sup> Beyond the near-term goal of rendering devices already known in the literature more mechanically stable, intrinsically elastic and ductile (“stretchable”) semiconductors could find applications in new types of systems, such as wearable and implantable biomedical sensors<sup>11</sup> and in soft robotics.<sup>12</sup> This paper represents an attempt to find the “best of both worlds”—i.e., to coengineer the mechanical compliance and photovoltaic efficiencies—in a series of P3ATs, the most-studied class of materials in the field of organic electronics.<sup>13</sup> The lengths of the alkyl side chains in P3ATs have very large effects on virtually all mechanical and electronic properties of the materials.<sup>1,5,14</sup> The largest increase in mechanical compliance occurs in a series of P3ATs having

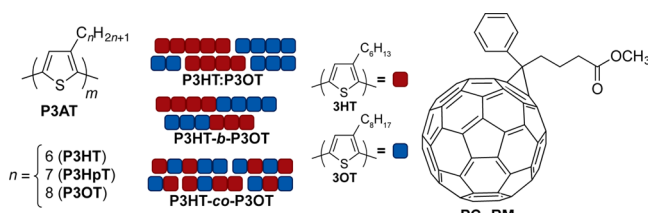
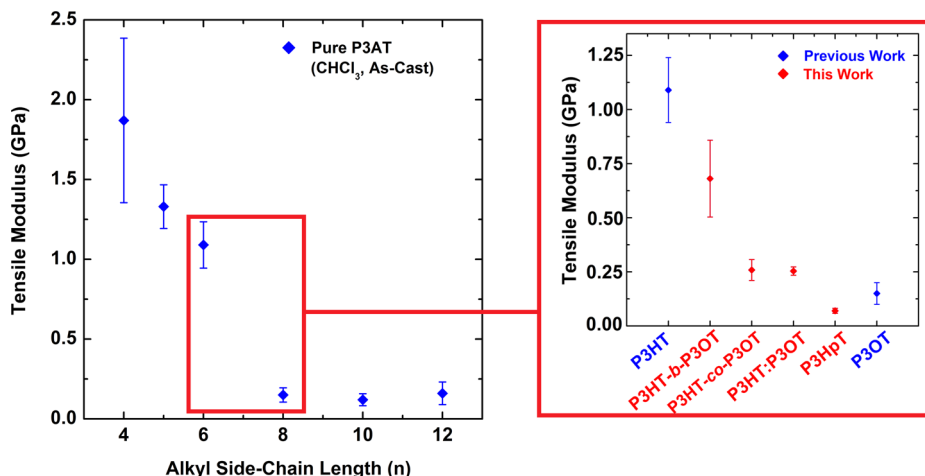


Figure 1. Chemical structures and schematic diagrams of the organic semiconductors examined in this paper.

2).<sup>1,2</sup> Several groups have reported a deleterious effect on the electronic and photovoltaic properties with increasing side-chain length, including field-effect mobilities<sup>5,6</sup> and power conversion efficiency (PCE) in bulk heterojunctions (BHJs) when paired with a polyfluorene copolymer<sup>7</sup> and fullerene derivative.<sup>8</sup> O’Connor and co-workers have reported a similar competition between field-effect mobilities and tensile moduli of various conjugated polymers.<sup>3</sup> This competition has been

Received: February 5, 2014

Revised: February 25, 2014



**Figure 2.** Plot of tensile modulus vs alkyl side-chain length. Tensile moduli of the pure polymer thin films spin-coated from chloroform were measured via buckling methodology. Materials examined for the first time are indicated in red. The “sweet spot” between  $n = 6$  and  $8$  is highlighted.

between six and eight carbon atoms—poly(3-hexylthiophene) (P3HT) and poly(3-octylthiophene) (P3OT). We thus sought to determine the effect of the length of alkyl side chain in the “sweet spot” on the elasticity and photovoltaic performance and to attempt to maximize the two parameters. Toward this goal, we obtained or synthesized a series of four materials exhibiting an average side-chain length of  $n = 7$ : (1) a physical blend (P3HT:P3OT); (2) a block copolymer (P3HT-*b*-P3OT); (3) a random copolymer (P3HT-*co*-P3OT); and (4) poly(3-heptylthiophene) (P3HpT), whose side chain contains exactly seven carbon atoms (Figure 1), and whose field effect mobility has been reported to be between those of P3HT and P3OT.<sup>6</sup>

**Plastic Electronics.** The vision of organic electronics has always been to fabricate traditional semiconductor devices using inexpensive materials that can be processed from solution in a roll-to-roll manner.<sup>15–17</sup> The thinness of the active layers ( $\leq 200$  nm) required to realize applications such as OSCs, OTFTs, and organic light-emitting devices (OLEDs) permits extremely small bending radii and substantial overall flexibility, as long as the device is fabricated on a sufficiently thin substrate (OSCs with a total thickness of  $2\ \mu\text{m}$  have been demonstrated).<sup>16</sup> The strains imposed on materials under bending are rarely  $>2\%$ , however, and for a material to accommodate substantial tensile strain for integration with ultrathin substrates,<sup>18</sup> textiles,<sup>19</sup> the moving parts of machines and portable devices,<sup>20</sup> medical prostheses and implants,<sup>11</sup> robotics,<sup>21</sup> and three-dimensional surfaces other than cones and cylinders,<sup>2</sup> significantly more mechanical robustness is required of these nominally plastic semiconductors.<sup>22</sup> The best-performing organic semiconductors—including pentacene, poly[2,5-bis(3-tetradecylthiophen-2-yl)thieno[3,2-*b*]thiophene] (PBTTT), and P3HT:PCBM blends—are stiff (elastic moduli  $> 1$  GPa) and brittle (crack-onset strain on elastomeric substrates  $< 2\%$ ).<sup>3,23,24</sup>

Electronic properties for organic electronic materials and devices have surpassed or are approaching those of their inorganic counterparts.<sup>25–27</sup> Semiconducting polymers now exhibit ambipolar field-effect mobilities greater than those of amorphous silicon,<sup>25</sup> and organic solar cells have reached efficiencies over ten percent.<sup>28</sup> Studies on roll-to-roll manufacturing suggest that modules can be made at low cost.<sup>29</sup> While some of the most impressive demonstrations have used high-mobility, low-bandgap polymers,<sup>30</sup> regioregular

P3HT is still the archetypal conjugated polymer and serves as a reference point for comparing the properties of new materials.<sup>13</sup> Even though the photovoltaic properties of structurally complex, donor–acceptor copolymers have surpassed those of P3HT (though perhaps not by much<sup>31</sup>), P3HT has significant advantages including synthetic accessibility<sup>32</sup> and low embodied energy,<sup>33</sup> facile functionalization by side-chain engineering,<sup>14</sup> amenability to block copolymerization,<sup>34</sup> and a band gap that is complementary to modern donor–acceptor copolymers for tandem cells.<sup>26</sup>

While the power conversion efficiency (PCE) is frequently the focal point for studies of organic solar cells, the mechanical resiliency is often overlooked. Despite its good photovoltaic performance under ideal conditions,<sup>31</sup> P3HT—especially when combined with PC<sub>61</sub>BM—has been shown to fracture at relatively low applied strains.<sup>1,4,23,24</sup> Our laboratory has shown that small changes in the structure of a conjugated polymer,<sup>35</sup> such as varying the length of the alkyl side chains, can significantly alter the electronic and mechanical properties of the poly(3-alkylthiophene)s (P3ATs).<sup>1,2</sup> For example, increasing the length of the side chain of P3AT from butyl to hexyl decreases the tensile modulus from 1.87 to 1.09 GPa; increasing it further to octyl decreases the modulus to 150 MPa (Figure 2).<sup>1</sup> The extreme compliance of P3OT—even in a blend with PCBM<sup>1</sup>—permits it to be strained to conform to hemispherical objects without wrinkling.<sup>2</sup> The elasticity and ductility of P3OT, however, come at a cost of significantly degraded field-effect mobility and photovoltaic efficiency compared to P3HT.<sup>2,5</sup>

Elasticity and ductility are regarded as antithetical to electronic performance; several studies are consistent with this perception. O’Connor et al. noted a correlation between stiffness and charge-carrier mobility in two types of polythiophenes, P3HT and PBTTT.<sup>3</sup> Intercalation of the side chains in the case of PBTTT led to good vertical registration and a highly crystalline morphology.<sup>3</sup> This ordered microstructure was correlated with good charge transport properties (although high crystallinity is not always a prerequisite for good photovoltaic performance<sup>36</sup>). Poor vertical registration in the case of P3HT, whose side chains are liquid-like at room temperature, produces a semicrystalline film that is relatively stretchable but has a field-effect mobility that is no longer considered state-of-the art.<sup>3</sup> In another system, Awartani et al.

showed that slow evaporation of the solvent during casting of P3HT:PC<sub>61</sub>BM blends led to greater order of the polymer (as determined by applying the weakly interacting H aggregate model to UV-vis spectra of the solid films)<sup>37</sup> and greater photovoltaic performance, but also greater stiffness and brittleness.<sup>4</sup> This paper explores the range in side-chain length between  $n = 6$  and  $n = 8$  (Figure 2) within which we postulated the existence of a “sweet spot” that maximizes mechanical resilience and photovoltaic performance. In particular, we compared the tensile moduli, structure as deduced by ultraviolet-visible (UV-vis) spectroscopy and atomic force microscopy (AFM), and photovoltaic properties (when blended with PC<sub>61</sub>BM) of the six polymeric samples shown in Figure 1.

## 2. EXPERIMENTAL DESIGN

**2.1. Selection of Materials. P3HT, P3OT, and P3HpT.** We chose P3HT because it is the most studied conjugated polymer for organic solar cells.<sup>13,26</sup> The photovoltaic performance of P3HT:PC<sub>61</sub>BM was used as the benchmark for the performance of all other tested organic photovoltaic devices. P3OT was selected for its low tensile modulus,<sup>1</sup> which is a necessary characteristic for polymers that are to be used in stretchable and flexible electronics. P3HpT was selected because the number of carbons in its alkyl side chain (seven) is the average of the number of carbons in the alkyl side chains of P3HT and P3OT. Our initial hypothesis was that the properties of P3HpT would be intermediate between those of P3HT and P3OT.<sup>6</sup>

**Block and Random Copolymers.** We also synthesized block and random copolymers having both hexyl and octyl side chains. Jenekhe and co-workers have measured differences in photovoltaic properties between physical blends of P3BT and P3OT and the covalently bonded block and random copolymers.<sup>38,39</sup> The authors found that the copolymers outperformed not only the physical blend, but also the homopolymers.<sup>38,39</sup> We expected that comparison of the properties of a physical blend, and block and random copolymers of P3HT and P3OT would provide insights into the relationship between molecular structure, morphology, and mechanical properties.

**2.2. Mechanical Characterization. Buckling-Based Metrology.** We measured two parameters—the tensile modulus and the crack onset strain—that permitted comparison of the elasticity and ductility of each thin film. The tensile moduli were measured using the mechanical buckling technique originally described by Stafford et al.<sup>40</sup> This method provides rapid quantitative measurements and is well suited for analyzing the mechanical properties for various thin-film systems including conjugated polymer films.<sup>1,4,23,24</sup> The technique relates the tensile modulus of the film to the quantitative description of the surface buckling pattern of the film under compressive strains on a relatively compliant substrate—as described originally by Hutchinson, Whitesides, and co-workers.<sup>41,42</sup> The advantages of using the buckling technique are 2-fold: (1) conventional mechanical testing devices typically lack the sensitivity to measure the forces involved in straining a thin film (and free-standing films  $\leq 100$  nm are difficult to handle and prepare);<sup>40</sup> (2) analysis using techniques that have adequate sensitivity such as nanoindentation may be complicated by effects of the substrate and by the viscoelasticity of some polymeric materials.<sup>43</sup> Briefly, the conjugated polymers were spin-coated onto passivated glass slides, then transferred to poly(dimethylsiloxane) (PDMS) substrates each bearing a small prestrain. After transfer, the PDMS substrates were relaxed; this action created a compressive strain that forced the conjugated polymer film to adopt sinusoidal buckles. The buckling wavelength,  $\lambda_b$ , and the thickness of the film,  $d_f$ , can be related to the tensile moduli of the film and the substrate,  $E_f$  and  $E_s$ , and the Poisson ratios of the two materials,  $\nu_f$  and  $\nu_s$  by the following equation:

$$E_f = 3E_s \left( \frac{1 - \nu_f^2}{1 - \nu_s^2} \right) \left( \frac{\lambda_b}{2\pi d_f} \right)^3 \quad (1)$$

We measured the tensile modulus of the substrate,  $E_s$  (using a commercial pull tester), the buckling wavelength,  $\lambda_b$  (by optical microscopy), and the film thickness,  $d_f$  (by stylus profilometry). The slope of a plot of  $\lambda_b$  vs  $d_f$  for three different film thicknesses was inserted into eq 1. The Poisson's ratios were taken as 0.5 and 0.35 for PDMS and the conjugated polymers films.<sup>1,23</sup> The experimental method is described in detail elsewhere.<sup>1</sup>

**Ductility.** Crack on-set strains have been shown to provide qualitative measure of the ductility of the thin polymer films,<sup>1,3,4</sup> with the caveat that poor adhesion of the P3AT to PDMS for long alkyl side chains ( $n > 8$ ) leads to increased apparent brittleness.<sup>1</sup> The propensity of the conjugated polymer films to form cracks when stretched on a compliant substrate was measured by transferring the film to the PDMS substrate bearing no prestrain, which was then stretched uniformly using a computer-controlled actuator. Optical micrographs of each film subjected to the strain of 1% to 80%, with a step size of 1%, were examined for the first sign of crack formation.

**2.3. Theoretical Determination of Tensile Modulus.** We attempted to compare the tensile moduli obtained experimentally to those calculated by a semiempirical theory that takes into account the chemical structure and thermal properties of the polymers. This approach was originally described by Seitz,<sup>44</sup> applied to conjugated polymers by Tahk et al.,<sup>23</sup> and then modified to account for differential glass transition temperatures between polymers.<sup>1</sup> The model successfully predicts the tensile moduli of pure polythiophenes and, in conjunction with composite theory, blends of conjugated polymers with fullerene derivatives.<sup>1,23</sup> However, this simple model does not account for the sequence of monomers within copolymers, and predicts, for example, the same tensile modulus for both block and random copolymers. A more sophisticated approach is necessary to describe these copolymers and is being pursued by us in a separate project.

**2.4. Fabrication of Devices.** We compared the photovoltaic properties of the various conjugated polymers using PC<sub>61</sub>BM as the electron acceptor. All conjugated polymer samples—P3HT, P3HpT, P3OT, the physical blend (P3HT:P3OT), the block copolymer (P3HT-*b*-P3OT), and the random copolymer (P3HT-*co*-P3OT)—were mixed with PC<sub>61</sub>BM in a 1:1 ratio. We deposited a layer of PEDOT:PSS containing 7% DMSO and 0.1% Zonyl fluorosurfactant as the transparent anode.<sup>45</sup> For the top contact, we used a liquid metal cathode, eutectic gallium–indium (EGaIn), extruded manually from a syringe. The use of EGaIn (work function 4.1–4.2 eV) has been reported in the literature to give similar results to those of devices comprising evaporated aluminum.<sup>46–48</sup> We chose EGaIn because it facilitated rapid characterization of our devices and because of our overarching interest in stretchable materials and devices, in which EGaIn is a ubiquitous stretchable conductor.<sup>49</sup>

**2.5. Weakly Interacting H Aggregate Model.** Order in films of semiconducting polymers is associated with both greater electronic performance and increased stiffness.<sup>3</sup> The extent of order, as determined by UV-vis spectroscopy, has been correlated to increased tensile moduli in P3HT:PCBM films.<sup>4</sup> Spano et al. and others have shown that aggregates of P3HT in solid films can be considered as weakly interacting H aggregates, due to cofacial  $\pi$ – $\pi$  stacking and weak excitonic coupling.<sup>4,37,50–53</sup> We used this model to compare trends in conjugation length from the UV-vis absorption spectra of the polymers, in an attempt to correlate these values with the mechanical stiffness and device performance. The model works as follows. Upon absorption of a photon, an electron is excited from the ground electronic state to an excited electronic state. In H aggregates, these electronic excitations are coupled with nuclear vibrations.<sup>37</sup> This coupling can be understood by a semiclassical picture, in which the nuclei of the polymer aggregates can be thought of as existing in potential wells with quantized vibrational levels, analogous to an electron trapped in a potential well.<sup>54</sup> At lower vibrational levels, the potential wells can be approximated as harmonic oscillators; in this approximation, the vibrational energy levels are equally spaced.<sup>37,54</sup> In conjugated molecules, such as P3ATs, the vibrational levels arise from the symmetric stretching and ring breathing of the C=C bonds.<sup>4,37,51,53</sup> When an electron is excited, the position of the

nuclear potential well in the excited state is shifted from the ground state and the electron and vibrational modes are therefore coupled.<sup>37</sup>

In the aggregated state (i.e., crystallites in solid films), these coupled electron-vibrational (vibronic) transitions determine the absorption of weakly interactive H aggregates and can be modeled as Gaussian fits by:<sup>4,37,50,51,53</sup>

$$A(E) \propto \sum_{m=0} \left( \frac{S^m}{m!} \right) \times \left( 1 - \frac{We^{-S}}{2E_p} \sum_{n \neq m} \frac{S^n}{n!(n-m)} \right)^2 \\ \times \exp \left( \frac{-\left( E - E_{00} - mE_p - \frac{1}{2}WS^m e^{-S} \right)^2}{2\sigma^2} \right) \quad (2)$$

In the above equation,  $A$  is the absorption by an aggregate as a function of the photon energy ( $E$ ).  $E_{00}$  is the energy of the  $0 \rightarrow 0$  vibronic transition, which is allowed assuming some disorder in the aggregates.<sup>37</sup>  $S$  is the Huang-Rhys factor, which quantifies the nuclear potential well shift upon vibronic transition from the ground state to the excited state.<sup>37</sup> It is calculated from absorption and emission spectra, and is set to 1 for P3ATs.<sup>37,51</sup>  $E_p$  is the intermolecular vibration energy, which (in the case where  $S = 1$ ) is the difference in energy between the vibrational levels in the excited state. It is set to 0.179 eV as determined by Raman spectroscopy.<sup>55</sup>  $W$  is the free exciton bandwidth, which is related to the nearest neighbor interchain excitonic coupling. Upon coupling, a dispersion of the energies occurs, the width of which is equal to  $W$  (which is four times the nearest neighbor coupling).<sup>37</sup>  $W$  is also inversely related to conjugation length; a lower  $W$  indicates better ordering of the aggregates.<sup>50</sup> The terms  $m$  and  $n$  are the ground- and excited state vibrational levels and  $\sigma$  is the Gaussian line width.

### 3. RESULTS AND DISCUSSION

**3.1. Characterization of the Polymers.** After synthesizing P3HT-*b*-P3OT and P3HT-*co*-P3OT, we examined the <sup>1</sup>H NMR spectra to estimate the ratios of 3HT and 3OT units in the polymers. Because the signals arising from the terminal methyl groups of the hexyl and octyl side chains were partially overlapped, we estimated the ratio of 3HT and 3OT units was the same as the molar ratios of the starting materials, approximately 1:1. The percent regioregularity for each sample was as follows: P3HT, 88%; P3HT-*b*-P3OT, 90%; P3HT-*co*-P3OT, 89%; P3Hpt, 92%; P3OT, 82%. While the mechanical properties of most polymeric materials exhibit dependency on the molecular weight, this effect tends to saturate at a sufficiently high molecular weight.<sup>56</sup> Our laboratory has shown that the difference in tensile moduli between the commercial sample of P3HT ( $M_w = 29\,000$  g mol<sup>-1</sup>, PDI = 2.0) and the sample synthesized in-house by the Grignard metathesis polymerization<sup>57</sup> ( $M_w = 7500$  g mol<sup>-1</sup>, PDI = 1.2) was minimal:  $1.09 \pm 0.15$  GPa for the commercial sample and  $1.05 \pm 0.35$  GPa for the sample synthesized in-house.<sup>2</sup> Dauskardt and co-workers also reported the dependency of the mechanical properties on molecular weight, and found similar storage and loss moduli for samples with  $M_w$  ranging from 28 000 to 100 000 g mol<sup>-1</sup> (samples with  $M_w < 28\,000$  g mol<sup>-1</sup> were not tested).<sup>58</sup> These data suggest that in the elastic regime,  $M_w$  does not significantly affect the tensile moduli for the values of  $M_w$  of P3AT samples typically reported in the literature. We assumed covalent connectivity of the blocks in P3HT-*b*-P3OT by following the same synthetic protocol as used in several previous studies on P3AT block copolymers, and by observation of a peak with a single retention time by gel permeation chromatography (GPC).<sup>38,59-62</sup>

**3.2. Mechanical Properties of Pure Polymer Films.** We began the characterization of the mechanical properties of each conjugated polymer by measuring the tensile modulus of the pure polymer film spin-coated from chloroform. In a previous report from our group, we measured decreasing moduli with increasing length of the alkyl side-chain in a series of P3ATs where A = butyl, hexyl, octyl, and dodecyl.<sup>1</sup> Figure 2 and Table 1 show the values obtained for the hybrid polymers on the

**Table 1. Tensile Moduli of Pure Polymers Spin-Coated from CHCl<sub>3</sub> As-Cast and Their Blends with PC<sub>6</sub>BM Spin-Coated from ODCB and Thermally Annealed at 100 °C**

materials	tensile modulus (GPa)	
	pure polymer (CHCl <sub>3</sub> , as-cast)	1:1 polymer:PC <sub>6</sub> BM (ODCB, annealed)
P3HT	$1.09 \pm 0.15^a$	$3.85 \pm 0.32$
P3HT- <i>b</i> -P3OT	$0.68 \pm 0.18$	$2.72 \pm 0.91$
P3HT- <i>co</i> -P3OT	$0.26 \pm 0.05$	$2.12 \pm 0.22$
P3HT:P3OT	$0.25 \pm 0.02$	$2.32 \pm 0.24$
P3Hpt	$0.07 \pm 0.01$	$1.79 \pm 0.35$
P3OT	$0.15 \pm 0.05^a$	$0.51 \pm 0.07$

<sup>a</sup>Values taken from ref 1.

same set of axes as those obtained in our previous study (we have since added pentyl and decyl to the plot for the purposes of this paper). The tensile moduli of the three individual polymer films containing both hexyl and octyl side chains—the block and random copolymers and the physical blend—lie in between those of the P3HT and P3OT, as expected; however, the tensile modulus of the block copolymer ( $680 \pm 180$  MPa) was determined to be almost three times those of the random copolymer ( $260 \pm 50$  MPa) and physical blend ( $250 \pm 20$  MPa), which were nearly identical. For all three samples, the molar concentration of the 3HT and 3OT units were approximately 1:1. We thus attributed the differences in moduli to unequal microstructures of the three samples in the solid state rather than solely from the ratio of total hexyl and octyl side chains in the samples. Previous work on polymer–polymer blends that exhibit some extent of mutual solubility suggested that the tensile modulus of the blend is the synergistic modulus (weighted average) of the two homopolymers. For example, in the blend of poly(ether ether ketone) (PEEK) and poly(aryl ether sulfone) (PES),<sup>63</sup> and a blend of poly(ether imide) (PEI) and poly(trimethylene terephthalate) (PTT),<sup>64</sup> the authors demonstrated that the tensile moduli of each blend can be plotted against the molar concentration of one of the components to yield a linear relationship. Interestingly, we observed that the modulus of the block copolymer (P3HT-*b*-P3OT) was close to the synergistic modulus, while the moduli of the random copolymer and physical blend lied below (Figure 3a). To determine if the differences in moduli were attributable to variations in surface morphology, we examined thin films of these polymers by AFM; the results for these experiments are discussed in section 3.5.

**Block Copolymer.** We attributed the higher value of the tensile modulus of the block copolymer to the covalent bonds between the P3HT and P3OT segments that promote the formation of connected crystalline domains comprising both P3HT and P3OT. Jenekhe and co-workers observed two distinct interchain (lamellar) spacings by grazing incidence X-ray diffraction (GIXD) in a block copolymer of P3BT ( $n = 4$ ) and P3OT of equal composition of monomers.<sup>38</sup> These two

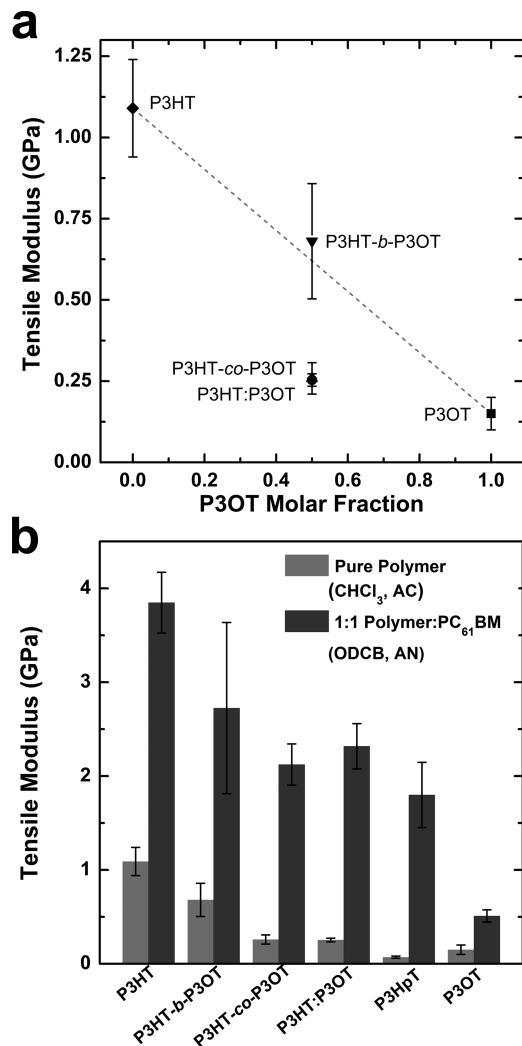


**Figure 3.** (a) Tensile moduli of polymer films containing both hexyl and octyl side chains along with the pure polymers. The dashed line shows the weighted average of the pure polymers. (b) Comparison between the pure polymer films spin-coated from chloroform (as-cast, AC) and the films comprising 1:1 polymer:PC<sub>61</sub>BM blends spin-coated from ODCB and thermally annealed at 100 °C (AN).

distinct signals corresponded to the lamellar spacings of the blocks of P3BT and P3OT.<sup>38</sup> We expected that P3HT-*b*-P3OT would behave similarly and form two distinct crystalline domains. Because the domains are covalently linked through the conjugated main chain, the more compliant P3OT phase is bound to the more rigid P3HT phase and thus the block copolymer is less able to accommodate strain than is the physical blend, P3HT:P3OT, discussed below.

**Random Copolymer.** Unlike P3HT-*b*-P3OT, P3HT-*co*-P3OT, which has statistically incorporated monomers, is not likely to form two distinct crystalline domains. In films of a similar copolymer, P3BT-*co*-P3OT, Jenekhe and co-workers observed a single type of crystalline domain whose lamellar spacing correlated with the ratio of the monomers.<sup>39</sup> The standard model for packing within P3HT crystallites assumes no interdigitation of side chains ("form I");<sup>65</sup> although interdigitation has been observed in the oligomer of 3HT with repeat units  $\leq 20$  ("form II").<sup>66</sup> The randomness in packing of side chains in the interlamellar regions, along with decreased registration between the lamellae, could contribute to

the tensile modulus that was lower for P3HT-*co*-P3OT than for P3HT-*b*-P3OT.

**Physical Blend.** Our next task was to understand the mechanical behavior of the physical blend of P3HT and P3OT (P3HT:P3OT). A tensile modulus for P3HT:P3OT that was lower than the synergistic modulus would be consistent with a blend in which the phases were at least partially separated. In phase-separated blends, the more compliant P3OT phase may accommodate the strain, thus rendering the modulus of the blend closer to that of P3OT. This behavior is in contrast to that of P3HT-*b*-P3OT, in which the covalent connectivity of the domains resists deformation of the film. We note that cocrystallization has been observed in P3HT:P3OT blends by Nandi and co-workers by observation of a single lamellar spacing by X-ray diffraction.<sup>67</sup> The authors found, however, that the tendency to cocrystallize was extremely sensitive to differences in both the ratio of the components and regioregularity between the two isolated polymers.<sup>67</sup>

**Poly(3-heptylthiophene).** The P3ATs are a class of comb-like polymers<sup>68</sup> whose properties represent a compromise between the rigid main chain and the paraffinic side chains. For many systems, a monotonic decrease in  $T_g$  accompanies increasing side-chain length,  $n$ , up to a critical side-chain length,  $n_c$ . The trend exhibits a discontinuity at  $n_c$ , and for  $n > n_c$ ,  $T_g$  changes little or even increases.<sup>69</sup> If one defines the critical alkyl side chain length in terms of the tensile modulus, then it appears that  $n_c = 7$  for P3ATs, even though  $T_g$  continues to decrease up to at least  $n = 12$ .<sup>70</sup> The observed modulus of P3H<sub>7</sub>T ( $70 \pm 10$  MPa) is within the same order of magnitude as that of P3OT and P3DDT (Figure 2).<sup>1</sup> Unlike the copolymers and the physical blend, the compliance of P3H<sub>7</sub>T cannot be a consequence of the interaction between monomers with different side chains. Our measurement of the modulus of poly(3-pentylthiophene) (P3PT,  $n = 5$ ) ( $1.33 \pm 0.14$  GPa) and its placement on the line connecting P3BT and P3HT suggest that the conspicuously low modulus of P3H<sub>7</sub>T is also not a manifestation of the odd number of carbon atoms in the side chain. While the overall reduction in modulus with increasing  $n$  is expected on the basis of a corresponding reduction in  $T_g$  and the dilution of volume fraction of the main-chain with increasing length of the alkyl side chains,<sup>1</sup> the sharp drop in modulus from  $n = 6$  to  $n = 7$  is nonetheless conspicuous. This drop in modulus is consistent with the fact that P3H<sub>7</sub>T is the P3AT with the shortest side chains whose  $T_g$  is extrapolated to be significantly below room temperature ( $T_g$  for P3HT has been measured in the range of 12–25 °C for P3HT and –14 °C for P3OT).<sup>4,71</sup> Our theoretical calculation of the tensile moduli using the molecular structure of the monomers<sup>1,23,35,44</sup> predicted a value for P3H<sub>7</sub>T ( $130 \pm 20$  MPa) that was close to the experimental value ( $70 \pm 10$  MPa). This simple model, however, was unable to predict the moduli for the hybrid polymer samples. We believe that its failure arises from its inability to incorporate the interaction between different polymer chains within the films and the distribution of the monomers in the backbones (in both block and random copolymers).

**Ductility.** While the theoretical model failed to predict the tensile moduli of the copolymers and the physical blend, the trend in the apparent brittleness agrees well with the experimental values. Our group and others have found that the tensile modulus of P3AT correlates with brittleness when stretched on a compliant substrate.<sup>1,3,4,24</sup> We measured the strain at which the first crack appeared on the surface of the

film (crack on-set strain) of pure polymer films, spin-coated from chloroform without annealing (as-cast, AC). We observed that thin films of P3HT-*b*-P3OT crack at much lower applied strains (8%) than those of P3HT:P3OT and P3HT-*co*-P3OT, whose crack on-set strains are similar (30% and 32% respectively). In addition, P3HpT was observed to have a high crack on-set strain (58%), which was similar to those of P3OT and P3DDT.<sup>1</sup>

**3.3. Mechanical Properties of Polymer:PC<sub>61</sub>BM Composites.** The presence of fillers has a strong influence on the mechanical properties of composite materials.<sup>1,24</sup> For bulk heterojunction solar cells, polymers are usually blended with fullerene derivatives (PC<sub>61</sub>BM or PC<sub>71</sub>BM) at a ratio by weight of 1:1 to 1:4 (polymer:fullerene).<sup>26,28</sup> We measured the moduli of polymer:PC<sub>61</sub>BM films in a 1:1 ratio, which were spin-coated from ODCB and thermally annealed (AN). All samples were annealed at the same temperature (100 °C) for consistency and to decouple the effect of temperature on the mechanical and electronic properties. Various studies have demonstrated that the addition of fullerenes to conjugated polymers produces composites that are stiffer and more brittle than are the pure polymers.<sup>1–3,23,24</sup> We have also previously shown that the moduli of 2:1 blends of P3AT:PC<sub>61</sub>BM (including P3BT, P3HT, P3OT, and P3DDT) are 2–3 times that of pure P3ATs.<sup>1</sup> The exact factor by which the blend is stiffer than the pure polymer, however, depends strongly on the identity of the polymer<sup>24</sup> and the processing conditions (e.g., as in fast-dried and slow-dried films).<sup>4</sup> A previous report showed that the increase in modulus of a P3HT:PC<sub>61</sub>BM film over that of the pure polymer was a factor of approximately 5, whereas the increase in modulus of DPPT-TT:PC<sub>61</sub>BM over the pure polymer was only 40%.<sup>24</sup> This behavior suggests that interaction between the polymer and the PC<sub>61</sub>BM additive depends heavily on the morphologies of the blend, including miscibility of the polymer and the fullerene,<sup>72</sup> intercalation of the fullerene molecules between the side chain of the polymer,<sup>73</sup> and possible formation of bimolecular crystallites.<sup>74</sup> Each of these effects would strongly influence the mechanical properties of the blended films, and we are investigating these effects separately. Figure 3b and Table 1 show the values of the tensile moduli of polymer blends with PC<sub>61</sub>BM. The P3AT:PC<sub>61</sub>BM composites are observed to have higher tensile moduli than the pure polymers for all cases. The value of P3HT:PC<sub>61</sub>BM reported here is similar to those reported previously in the literature.<sup>23,24</sup>

**3.4. Photovoltaic Properties.** We fabricated photovoltaic devices by mixing the polymers in a 1:1 ratio with PC<sub>61</sub>BM. PEDOT:PSS was used as the transparent anode and eutectic gallium–indium (EGaIn) as the cathode.<sup>46</sup> Figure 4a shows the current density vs voltage (*J*–*V*) plots for the devices based on P3AT homopolymers. The P3HT:PC<sub>61</sub>BM (PCE = 2.04 ± 0.27%, N = 8) and P3OT:PC<sub>61</sub>BM (PCE = 0.67 ± 0.06%, N = 7) devices performed as expected relative to each other and the results agree with previously published results.<sup>8</sup> The P3OT:PC<sub>61</sub>BM devices performed poorly due to the low short-circuit current (*J*<sub>sc</sub>), 2.71 ± 0.32 mA cm<sup>−2</sup>, and fill factor (FF), 43.7 ± 1.0%. Surprisingly, the performance of P3HpT:PC<sub>61</sub>BM (PCE = 2.16 ± 0.17%, N = 8) did not fall between these values. Compared to P3HT:PC<sub>61</sub>BM, these devices had a similar *J*<sub>sc</sub> (6.95 ± 0.91 for P3HT:PC<sub>61</sub>BM vs 6.27 ± 0.48 mA cm<sup>−2</sup> for P3HpT:PC<sub>61</sub>BM), open circuit voltage (*V*<sub>oc</sub>) (568 ± 9 vs 598 ± 5 mV), and FF (51.7 ± 1.9 vs 57.5 ± 1.8%).

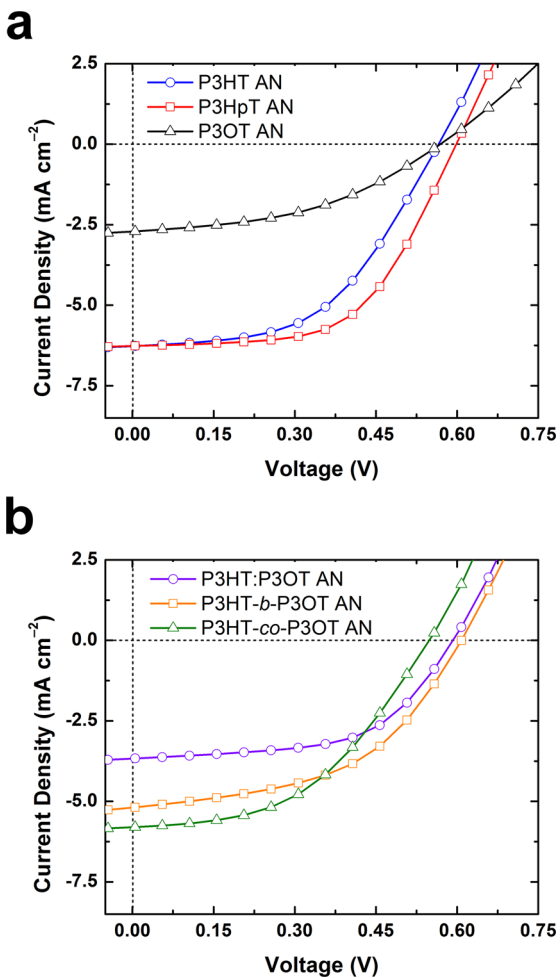


**Figure 4.** *J*–*V* curves of average devices ( $N \geq 7$ ) with an active layer of 1:1 blend of polymer and PC<sub>61</sub>BM. The architecture of the devices was PEDOT:PSS/polymer:PC<sub>61</sub>BM/EGaIn.

The *J*–*V* plots for the blended and copolymer devices are shown in Figure 4b. Among these polymers, the physical blend P3HT:P3OT:PC<sub>61</sub>BM (PCE = 1.24 ± 0.21%, N = 7) performed the poorest, while P3HT-*b*-P3OT:PC<sub>61</sub>BM (PCE = 1.56 ± 0.25%, N = 8) and P3HT-*co*-P3OT:PC<sub>61</sub>BM (PCE = 1.50 ± 0.19%, N = 7) performed similarly. The poor performance of the physical blend devices is likely due to their much lower *J*<sub>sc</sub> ( $3.67 \pm 0.56$  mA cm<sup>−2</sup>) compared to P3HT-*b*-P3OT:PC<sub>61</sub>BM ( $5.80 \pm 0.58$  mA cm<sup>−2</sup>) and P3HT-*co*-P3OT:PC<sub>61</sub>BM ( $5.19 \pm 0.76$  mA cm<sup>−2</sup>). The reduced *J*<sub>sc</sub> in the physical blend devices is attributed to the incorporation of P3OT phases, which have a low *J*<sub>sc</sub> as shown in the homopolymers devices. The photovoltaic properties for all devices tested are summarized in Table 2.

**3.5. Microstructural Characterization of the Polymer Films. AFM Analysis.** To determine if the mechanical and photovoltaic properties were due to differences in the morphologies of the films, films of the pure polymers were characterized by atomic force microscopy (AFM). We characterized both as-cast films and films annealed at 100 °C. Figure 5 shows the phase images obtained by AFM for these films. Fibril structures were observed in all as-cast films except for P3OT. Upon annealing, there was an increase in the phase contrast, which is indicative of an increase in order,<sup>75</sup> for all of the polymers except for P3HT-*b*-P3OT and P3HT-*co*-P3OT.

**Table 2. Summary of the Averaged  $J_{sc}$  (Short-Circuit Current),  $V_{oc}$  (Open-Circuit Voltage), FF (Fill Factor), and PCE (Power Conversion Efficiency) for the Solar Cells Fabricated in This Work ( $N \geq 7$ )<sup>a</sup>**

materials	$J_{sc}$ (mA cm <sup>-2</sup> )	$V_{oc}$ (mV)	FF (%)	PCE (%)
P3HT	6.95 ± 0.91	568 ± 9	51.7 ± 1.9	2.04 ± 0.27
P3HpT	6.27 ± 0.48	598 ± 5	57.5 ± 1.8	2.16 ± 0.17
P3OT	2.71 ± 0.32	570 ± 14	43.7 ± 1.0	0.67 ± 0.06
P3HT:P3OT	3.67 ± 0.56	592 ± 11	57.0 ± 1.6	1.24 ± 0.21
P3HT- <i>b</i> -P3OT	5.19 ± 0.76	607 ± 5	49.4 ± 0.5	1.56 ± 0.25
P3HT- <i>co</i> -P3OT	5.80 ± 0.58	549 ± 9	47.0 ± 1.6	1.50 ± 0.19

<sup>a</sup>The solar device architecture was PEDOT:PSS/polymer:PC<sub>61</sub>BM/EGaIn. The active layer was spin-coated from a solution of 1:1 polymer:PC<sub>61</sub>BM in ODCB (40 mg mL<sup>-1</sup>). To ensure the preparation of solar devices was consistent with the preparation of samples for mechanical testing, all devices were annealed at 100 °C in an inert atmosphere.

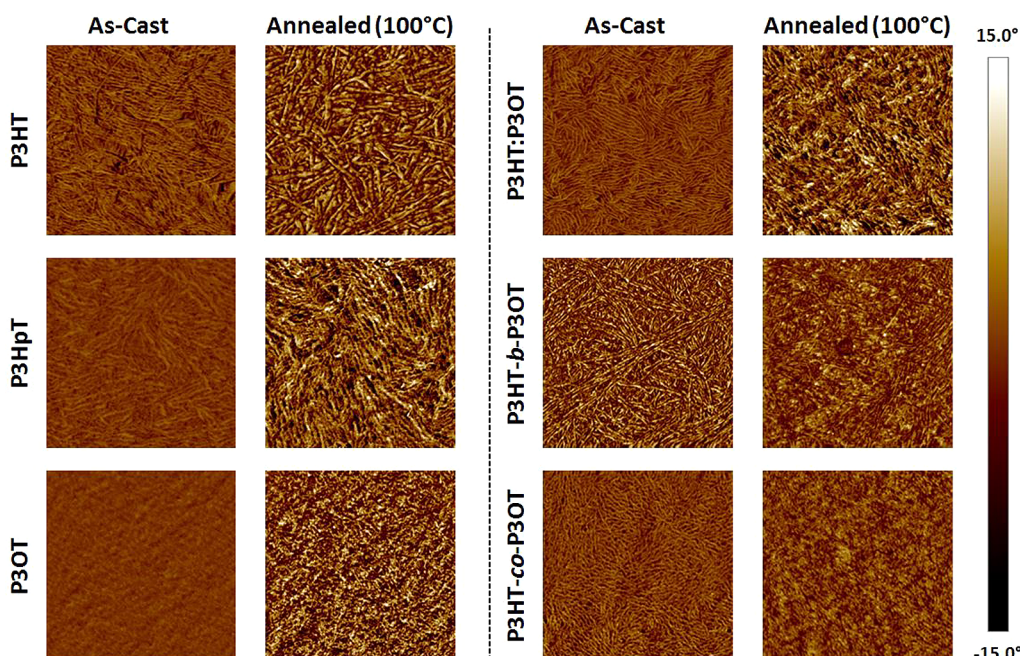


**Figure 5.** Phase images of pure polymers spin-coated from ODCB both as-cast and annealed. The dimensions are 1.5 μm × 1.5 μm.

The increase in order demonstrated by pure polymers and the physical blend was expected, but the apparent lack of further ordering in the P3HT-*b*-P3OT and P3HT-*co*-P3OT films was surprising. The covalent connectivity of the copolymers might suppress a change in microstructure that is large enough to be visible by AFM. For a finer-grained analysis of the evolution in microstructure with annealing, we turned to UV-vis spectrophotometry.

**UV-Vis Spectrophotometry.** To extract information about the relative conjugation lengths of the pure polymers, we characterized them by UV-vis spectrophotometry. The polymers were spin-coated onto glass out of chloroform and the absorption of the films was measured over the range 1.46–4.13 eV ( $\lambda = 850$ –300 nm). The UV-vis spectra of the homopolymers are shown in Figure 6, parts a and b, and those of the polymer blend and copolymers are shown in Figure 6, parts c and d. The polymers represented in Figure 6, parts a and c, were unannealed, while those represented in Figure 6, parts b and d, were after annealing at 100 °C in an inert atmosphere. Two observations can be made from visual inspection of these absorption curves. First, all of the curves for the annealed polymer films have better defined shoulders than their unannealed counterparts. The increase in definition of the shoulders indicates an increase in order in the polymer films

upon annealing.<sup>4,37,50–53</sup> Second, after annealing, P3HT and P3HpT have very similar absorption curves, which implies similar electronic structures and order in the solid film. The absorption curve of P3OT suggests less ordering. The annealed P3HT-*b*-P3OT and P3HT:P3OT samples also have very similar absorption curves which are consistent with similarly ordered crystallites in the films. Jenehke and co-workers have previously shown that block copolymers of P3BT and P3OT form distinct domains of each polymer.<sup>76</sup> From our analysis, we believe that our samples of P3HT-*b*-P3OT and P3HT:P3OT likely form distinct crystallites of P3HT and P3OT, as these materials have UV-vis spectra that essentially overlap with the superposition of the pure P3HT and P3OT films.

To explore further the effects of annealing on the polymer films, we utilized the weakly interacting H aggregate model. The absorption spectrum of P3HT, and by extension other P3ATs, can be envisioned as a superposition of the absorption by polymer crystallites and the absorption by the regions of amorphous polymer. The absorption by crystallites dominates the lower energy region, while the absorption at higher energies occurs predominantly by the amorphous polymer.<sup>4</sup> The weakly interacting H aggregate model was used to deconvolute the absorption spectra and determine the absorption by the polymer aggregates. From this model, we attempted to

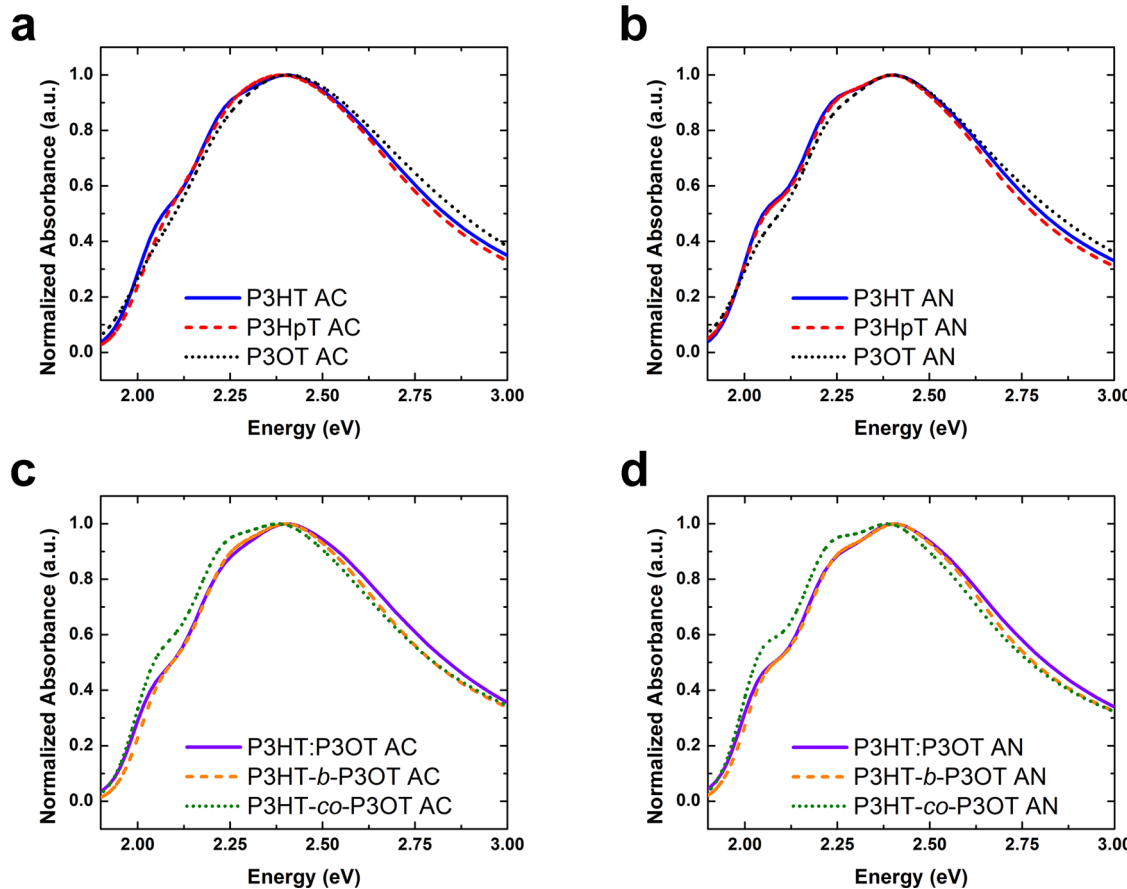


**Figure 6.** Absorption of polymer thin films cast from CHCl<sub>3</sub>. (a) Homopolymers as-cast (AC). (b) Homopolymers annealed at 100 °C in an inert atmosphere (AN). (c) Blend and copolymers as-cast (AC). (d) Blend and copolymers annealed at 100 °C in an inert atmosphere (AN).

correlate the conjugation length (from the exciton bandwidth) to mechanical stiffness and device performance. With the Huang–Rhys factor,  $S$ , set to 1, the exciton bandwidth,  $W$ , can be calculated from the approximated expression<sup>50</sup>

$$\frac{A_{0-0}}{A_{0-1}} \approx \left( \frac{1 - 0.24W/E_p}{1 + 0.073W/E_p} \right)^2 \quad (3)$$

where  $A_{0-0}$  and  $A_{0-1}$  are the absorption intensities of photons with the energies of the 0→0 and 0→1 vibronic transitions, respectively. Qualitatively, a decrease in the ratio of  $A_{0-0}$  to  $A_{0-1}$  is related to an increase in local order.<sup>4,37,50</sup> More specifically,  $W$  is inversely related to conjugation length and order; a lower  $W$  is indicative of a longer conjugation length and better order.<sup>50</sup>

The energy of the 0→0 vibronic transition,  $E_{00}$ , was found by calculating the second derivative of the absorption curves using a Matlab program. The same procedure was repeated to find the energy of the 0→1 vibronic transition. The absorption at these energies was then used to calculate the exciton bandwidth,  $W$  from eq 3. The Gaussian line width,  $\sigma$ , and the scaling factor for the calculated absorption were then found by a least-squares fit to the experimental absorption in the region of 1.93 to 2.25 eV.<sup>4,53,77</sup> This region was selected because the absorption is dominated by the polymer aggregates. Above 2.30 eV, the amorphous polymer dominates absorption.<sup>51,77</sup> The results are summarized in Table 3.

Among the homopolymers cast from chloroform after annealing, we found that the inverse of  $W$ , and thus conjugation

**Table 3. Summary of the Weakly Interacting H Aggregate Model Parameters for the Polymers in This Work<sup>a</sup>**

materials	$W$ (eV)	$1/W$ (eV <sup>-1</sup> )	$\sigma$ (eV)	$E_{00}$ (eV)	$\lambda_{E00}$ (nm)
P3HT	0.160	6.250	0.079	2.043	607
P3HpT	0.158	6.335	0.081	2.050	605
P3OT	0.189	5.278	0.091	2.039	608
P3HT:P3OT	0.174	5.762	0.079	2.036	609
P3HT-b-P3OT	0.169	5.922	0.079	2.050	605
P3HT-co-P3OT	0.145	6.889	0.077	2.039	608

<sup>a</sup>All materials were cast from CHCl<sub>3</sub> and then annealed at 100 °C in an inert atmosphere.

length, of P3HT is similar to P3HpT and greater than P3OT. These values agree with our observations of the materials in our photovoltaic measurements and suggest that a contributing factor for poor device performance in P3OT is a shorter conjugation length than P3HT (and P3HpT). The conjugation length also appears to fit the trend (but not as strongly) of the tensile moduli of the materials. The first work that correlated order in these materials obtained from UV-vis spectra to mechanical properties was that of Awartani et al.<sup>4</sup>

**3.6. Correlations between Tensile Modulus and Photovoltaic Performance.** We began our investigation motivated by our observations and those of others that mechanical compliance and electronic performance of organic semiconductors were apparently in competition. Our analysis of four conjugated polymer samples with characteristics that represented different methods of hybridizing P3HT (stiff but

good electronic properties) and P3OT (compliant but poor electronic properties) revealed P3HpT as the material that best combined both mechanical compliance and photovoltaic performance. In particular, the similarities of the photovoltaic properties and the order as measured by UV-vis spectroscopy and the weakly interacting H aggregate model are largely manifestations of the crystalline regions in a polymer film, which were of similar extent in both P3HT and P3HpT. The mechanical properties for a material operating above its  $T_g$ , however, are largely manifestations of the amorphous regions of a polymer. The relatively long side chains of P3HpT and P3OT tend to suppress  $T_g$  well below room temperature, and provide increased elasticity and ductility compared to P3HT. The effect of blending PC<sub>61</sub>BM into polymers to form bulk heterojunctions is to increase the modulus of the polymer:fullerene composite relative to that of the pure polymer. Because the fullerenes exist in fullerene-rich and mixed phases (they do not intercalate into the crystalline phases of P3ATs), the increase in modulus is most likely dependent on the solubility of the fullerene in the amorphous regions of the polymer, which in turn depends at minimum on the length of the alkyl side chain. While the field has recently achieved an impressive model of the morphology of the bulk heterojunction,<sup>78–80</sup> additional work will be required to develop a composite theory that predicts accurately the mechanical properties of these types of blends. Figure 7 presents our best evidence that combining

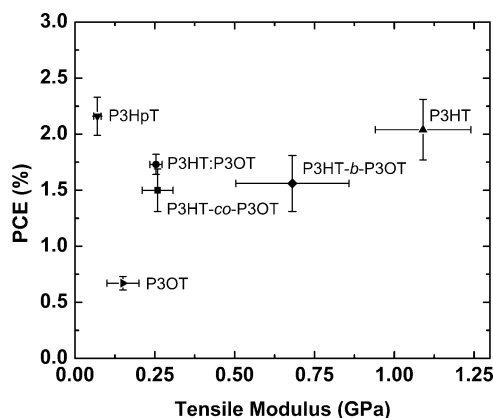


**Figure 7.** Plot of power conversion efficiency of the polymers in a 1:1 blend with PC<sub>61</sub>BM vs tensile moduli of the pure polymers. The position of P3HpT well above and to the left of the line connecting P3HT and P3OT suggest that in principle it is possible to coengineer mechanical and photovoltaic properties in a single material.

mechanical compliance and electronic performance in the same material is possible in principle. That is, P3HpT lies in the extreme corner of the quadrant that combines favorable mechanical and electronic properties, as manifested in good photovoltaic properties in blends with fullerenes. While the P3HpT:PC<sub>61</sub>BM blend is considerably stiffer than is the pure polymer, PC<sub>61</sub>BM is not the only acceptor that can be used in organic solar cells; it is likely that blending P3ATs with other acceptors will produce composites with mechanical properties that are far different from polymer:fullerene blends.

#### 4. CONCLUSION

This paper described our efforts to synthesize or discover a conjugated polymer that exhibited high values of mechanical compliance and electronic performance manifested in good

photovoltaic properties using P3ATs as the model organic semiconductor. We discovered a very large effect of the alkyl side chain (between six and eight carbon atoms) in determining the mechanical and electronic properties. In particular, we found that polythiophene with side chains containing seven carbon atoms, P3HpT, exhibited the optimal combination of mechanical compliance and photovoltaic efficiency. Examination of the mechanical and photovoltaic properties of the block and random copolymers and a physical blend of P3HT and P3OT revealed that the block copolymer exhibited the synergistic (average) modulus, while the random copolymer and physical blend did not.

Our findings may provide insights toward the design and synthesis of organic semiconductors that combine state-of-the-art electronic properties with extreme softness. It also highlights the critical role played by small changes (from six to seven carbon atoms in the alkyl side chain) in determining the bulk and electronic properties of these materials. Our work on copolymers exposed the shortcoming in a common semi-empirical approach to predicting the moduli of semiconducting polymers in its inability to differentiate the spatial distribution of unlike monomers (block vs random copolymers with identical mole fractions of the components). Understanding of the role of chemical structure on the mechanical properties of organic semiconductors could lead the way toward truly multifunctional materials with tunable properties.

#### 5. EXPERIMENTAL METHODS

**5.1. Materials.** Poly(3-pentylthiophene), poly(3-heptylthiophene), and poly(3-decylthiophene) were purchased from Rieke Metals, Inc., and used as received. Poly(3-hexylthiophene) and poly(3-octylthiophene) were purchased from Sigma-Aldrich and used as received. 3-Hexylthiophene and 3-octylthiophene were purchased from TCI and used as received. Dichlorobistriphenylphosphinopropane nickel(II) was purchased from Strem. [6,6]-phenyl C<sub>61</sub> butyric acid methyl ester (PC<sub>61</sub>BM) was obtained from Sigma-Aldrich with >99% purity. PDMS, Sylgard 184 (Dow Corning), was prepared according to the manufacturer's instructions at a ratio of 10:1 (base:cross-linker) and cured at room temperature for 36 to 48 h before it was used for mechanical testing. (Tridecafluoro-1,1,2,2-tetrahydrooctyl)-1-trichlorosilane (FOTS) was obtained from Gelest. PEDOT:PSS (Clevios PH1000) was purchased from Heraeus. DMSO was purchased from BDH with purity of 99.9% and Zonyl (FS-300) fluorosurfactant were purchased from Sigma-Aldrich. All reagents were obtained from commercial suppliers and used without purification. Chloroform (CHCl<sub>3</sub>), ortho-dichlorobenzene (ODCB), acetone, isopropyl alcohol (IPA), methanol, hexanes, and tetrahydrofuran (THF) were obtained from Sigma-Aldrich and used as received. Determination of molecular weight of the block and random copolymers was performed by gel-permeation chromatography (GPC) using polystyrene standards. The Mn reported by the manufacturers for P3HT, P3HpT, P3DT, and P3OT were 44, 35, 40, and 34 kDa, respectively.

**5.2. Synthesis of Block and Random Copolymers.** P3HT-*b*-P3OT. Poly(3-octylthiophene)-block-poly(3-hexylthiophene) (P3OT-*b*-P3HT, "block"). In the first round-bottom flask (flask A), a solution of 2,5-dibromo-3-octylthiophene (2.00 g, 5.65 mmol) was prepared in THF (60 mL) at ambient temperature. To this solution was added an isopropyl magnesium chloride-lithium chloride complex (4.5 mL of a 1.3 M solution in THF, 5.65 mmol). A suspension of Ni(dppp)Cl<sub>2</sub> (61 mg, 0.113 mmol, in 10 mL THF) was added by syringe in one portion. The polymerization proceeded to produce a dark red solution that fluoresced red-orange when illuminated with a long-wave ultraviolet lamp. This reaction was allowed to proceed for 10 min. Meanwhile, in a separate round-bottom flask (flask B), a solution of 2,5-dibromo-3-hexylthiophene (1.84 g, 5.65 mmol) was prepared in THF (60 mL). This solution was treated with an isopropyl magnesium chloride-lithium chloride complex (4.5 mL of a 1.3 M solution in THF, 5.65

mmol). After the 10 min reaction time in flask A, the contents of flask B were added to flask A by syringe. The combined solution was allowed to stir for 3 h. The reaction mixture was quenched by pouring into 400 mL of methanol. The quenched mixture was poured into centrifuge tubes, spun at 2.5 k rpm, and decanted. The pellets were combined, placed on filter paper, and inserted into a Soxhlet extractor. The material was washed with methanol and hexanes, and extracted with chloroform. The chloroform fraction was concentrated in vacuo to give 562 mg (16% yield) of a red solid.  $^1\text{H}$  NMR (300 MHz,  $\text{CDCl}_3$ ):  $\delta$  (ppm) = 7 (s, 1H), 2.92–2.45 (br, 2H), 1.82–1.63 (br, 2H), 1.54–1.23 (br ovlp, 8H), 0.94 (t ovlp, approximately 1.5H), 0.91 (t ovlp, approximately 1.5H). As determined by GPC,  $M_n$  = 7 kDa and PDI = 1.48.

**P3HT-co-P3OT.** Poly(3-octylthiophene)-co-poly(3-hexylthiophene) (P3OT-co-P3HT, “random”). In a round-bottom flask, a solution of 2,5-dibromo-3-octylthiophene (2.00 g, 5.65 mmol) and 2,5-dibromo-3-hexylthiophene (1.84 g, 5.65 mmol) was prepared in THF (120 mL) at ambient temperature. To this solution was added an isopropyl magnesium chloride-lithium chloride complex (9.0 mL of a 1.3 M solution in THF, 11.3 mmol). A suspension of  $\text{Ni}(\text{dppp})\text{Cl}_2$  (122 mg, 0.113 mmol, in 10 mL THF) was added by syringe in one portion. The reaction was allowed to stir for 3 h, then quenched and purified in the manner described for the block copolymer. The chloroform fraction was concentrated in vacuo to give 693 mg (18% yield) of a red solid.  $^1\text{H}$  NMR (300 MHz,  $\text{CDCl}_3$ ):  $\delta$  (ppm) = 7 (s, 1H), 2.92–2.45 (br, 2H), 1.82–1.63 (br, 2H), 1.54–1.23 (br ovlp, 8H), 0.94 (t ovlp, approximately 1.5H), 0.91 (t ovlp, approximately 1.5H). As determined by GPC,  $M_n$  = 17 kDa and PDI = 1.55.

**5.3. Preparation of Substrates.** Glass slides used as substrates for solar devices were cut into 1-in squares with a diamond-tipped scribe. They were then subsequently cleaned with Alconox solution ( $2 \text{ mg mL}^{-1}$ ), deionized water, acetone, and then isopropyl alcohol (IPA) in an ultrasonic bath for 10 min each and then rinsed and dried with compressed air. Next, the glass was plasma treated at  $\sim 30 \text{ W}$  for 3 min at a base pressure of 200 mTorr ambient air to remove residual organic material and activate the surface.

Glass slides used as substrates for thin films for UV-vis spectrophotometry measurements were cut into 1-in squares with a diamond-tipped scribe. The slides were then rinsed with water and ultrasonicated in IPA for 20 min. The slides were then rinsed with IPA and dried by compressed air. Next the glass was plasma treated as described above. Blanks used to subtract the absorption of the glass were cleaned in the same manner.

Silicon substrates used for AFM measurements were cut into 1-cm<sup>2</sup> pieces. To remove debris from the surfaces, the silicon substrates were ultrasonicated in acetone for 10 min, followed by IPA for 10 min and subsequently rinsed with IPA and then dried with compressed air. The wafers were then plasma treated as described above.

**5.4. Preparation of Polymer Solutions.** Solutions of P3HT, P3HpT, P3OT, and hybrid materials of P3HT and P3OT (physical blend, random copolymer, and block copolymer) in  $\text{CHCl}_3$  ( $15 \text{ mg mL}^{-1}$ ) were prepared for the buckling technique and UV-vis. Solutions of the polymers in ODCB ( $20 \text{ mg mL}^{-1}$ ) were prepared for AFM, and 1:1 polymer:PC<sub>61</sub>BM solutions in ODCB ( $40 \text{ mg mL}^{-1}$ ) were prepared for solar cells. All solutions were allowed to stir overnight and filtered with a 1- $\mu\text{m}$  glass microfiber (GMF) syringe filter immediately before being spin-coated onto glass or silicon substrates.

**5.5. Fabrication of Solar Cells.** We deposited a layer of PEDOT:PSS from an aqueous solution containing 92.9 wt % Clevios PH 1000 ( $\sim 0.9$ –1.2 wt % PEDOT:PSS), 7.0 wt % DMSO, and 0.1 wt % Zonyl fluorosurfactant as the transparent anode. The solution was filtered with a 1- $\mu\text{m}$  glass microfiber syringe filter and then spin-coated at a speed of 500 rpm (250 rpm  $\text{s}^{-1}$  ramp) for 60 s, followed by 2000 rpm (750 rpm  $\text{s}^{-1}$  ramp) for 60 s. The samples were subsequently dried at 150 °C for 30 min. The photoactive layer was then spin-coated onto the electrode layer at a speed of 500 rpm (250 rpm  $\text{s}^{-1}$  ramp) for 240 s, followed by 2000 rpm (750 rpm  $\text{s}^{-1}$  ramp) for 60 s. A thin strip of the PEDOT:PSS electrode was exposed by wiping away some of the photoactive layer with chloroform so that electrical

contact could be made. The samples were then immediately placed in a nitrogen-filled glovebox and annealed at 100 °C for 30 min. The substrates were then allowed to cool slowly to room temperature. EGaIn (extruded by hand from a syringe) was used as the top contact. The photovoltaic properties were measured in a nitrogen-filled glovebox using a solar simulator with a 100 mW cm<sup>-2</sup> flux that approximated the solar spectrum under AM 1.5G conditions (ABET Technologies 11016-U up-facing unit calibrated with a reference cell with a KG5 filter). The current density versus voltage was measured for both dark and under illumination using a Keithley 2400 SourceMeter.

**5.6. Characterization of Materials.** The absorbance of the materials was measured using a PerkinElmer Lambda 1050 UV-vis-NIR spectrophotometer. The wavelength range measured was 850–300 nm with a step size of 1 nm. The polymer solutions were spin-coated onto the glass slides at a spin speed of 500 rpm (250 rpm  $\text{s}^{-1}$  ramp) for 240 s followed by 2000 rpm (750 rpm  $\text{s}^{-1}$  ramp) for 60 s. For each solution, two films were prepared. The first film was left as-cast and the second film was immediately placed in a nitrogen-filled glovebox and annealed at 100 °C for 30 min under a Pyrex petri dish covered in aluminum foil. After 30 min, the samples were allowed to slowly cool back down to room temperature.

Atomic force microscopy (AFM) micrographs were taken using a Veeco Scanning Probe Microscope in tapping mode. Data was analyzed with NanoScope Analysis v1.40 software (Bruker Corp.). The samples were prepared in the same manner as the samples for UV-vis, except the substrates used were Si pieces.

All compounds were characterized by  $^1\text{H}$  NMR (300 MHz, Varian) using  $\text{CDCl}_3$  as the solvent. The residual chloroform peak at 7.26 ppm was used to calibrate the chemical shifts.

## ■ AUTHOR INFORMATION

### Corresponding Author

\*(D.J.L.) E-mail: dlipomi@ucsd.edu.

### Author Contributions

<sup>†</sup>Equal contributions.

### Notes

The authors declare no competing financial interest.

## ■ ACKNOWLEDGMENTS

This work was supported by the Air Force Office of Scientific Research (AFOSR) Young Investigator Program, Grant Number FA9550-13-1-0156. Additional support was provided by the National Science Foundation Graduate Research Fellowship under Grant No. DGE-1144086, awarded to S.S., by the Initiative for Maximizing Student Development awarded to D.R., and by laboratory startup funds from the University of California, San Diego. The authors thank Prof. Brendan O’Connor, Prof. Frank Spano, and Prof. Paul Smith for helpful discussions.

## ■ REFERENCES

- (1) Savagatrup, S.; Makaram, A. S.; Burke, D. J.; Lipomi, D. J. *Adv. Funct. Mater.* **2014**, *24*, 1169–1181.
- (2) O’Connor, T. F.; Zaretski, A. V.; Shiravi, B. A.; Savagatrup, S.; Printz, A. D.; Diaz, M. I.; Lipomi, D. J. *Energy Environ. Sci.* **2014**, *7*, 370–378.
- (3) O’Connor, B.; Chan, E. P.; Chan, C.; Conrad, B. R.; Richter, L. J.; Kline, R. J.; Heeney, M.; McCulloch, I.; Soles, C. L.; DeLongchamp, D. M. *ACS Nano* **2010**, *4*, 7538.
- (4) Awartani, O.; Lemanski, B. I.; Ro, H. W.; Richter, L. J.; DeLongchamp, D. M.; O’Connor, B. T. *Adv. Energy. Mater.* **2013**, *3*, 399–406.
- (5) Babel, A.; Jenekhe, S. *Synth. Met.* **2005**, *148*, 169–173.

- (6) Salammal, S. T.; Mikayelyan, E.; Grigorian, S.; Pietsch, U.; Koenen, N.; Scherf, U.; Kayunkid, N.; Brinkmann, M. *Macromolecules* **2012**, *45*, 5575.
- (7) Friedel, B.; McNeill, C.; Greenham, N. *Chem. Mater.* **2010**, *22*, 3389–3398.
- (8) Nguyen, L. H.; Hoppe, H.; Erb, T.; Günes, S.; Gobsch, G.; Sariciftci, N. S. *Adv. Funct. Mater.* **2007**, *17*, 1071–1078.
- (9) Dupont, S. R.; Voroshazi, E.; Heremans, P.; Dauskardt, R. H. *Org. Electron.* **2013**, *14*, 1262–1270.
- (10) Sokolov, A. N.; Cao, Y.; Johnson, O. B.; Bao, Z. *Adv. Funct. Mater.* **2012**, *22*, 175–183.
- (11) Ghezzi, D.; Antognazza, M. R.; Maccarone, R.; Bellani, S.; Lanzarini, E.; Martino, N.; Mete, M.; Perile, G.; Bisti, S.; Lanzani, G.; Benfenati, F. *Nat. Photon.* **2013**, *7*, 400–406.
- (12) Ilievski, F.; Mazzeo, A. D.; Shepherd, R. F.; Chen, X.; Whitesides, G. M. *Angew. Chem., Int. Ed.* **2011**, *50*, 1890–1895.
- (13) Brinkmann, M. *J. Polym. Sci., Part B: Polym. Phys.* **2011**, *49*, 1218–1233.
- (14) Mei, J.; Bao, Z. *Chem. Mater.* **2014**, *26*, 604–615.
- (15) Krebs, F.; Gevorgyan, S.; Alstrup, J. *J. Mater. Chem.* **2009**, *19*, 5442.
- (16) Kaltenbrunner, M.; White, M. S.; Glowacki, E. D.; Sekitani, T.; Someya, T.; Sariciftci, N. S.; Bauer, S. *Nat. Commun.* **2012**, *3*, 770.
- (17) Rogers, J. A.; Someya, T.; Huang, Y. *Science* **2010**, *327*, 1603.
- (18) Kaltenbrunner, M.; Sekitani, T.; Reeder, J.; Yokota, T.; Kuribara, K.; Tokuhara, T.; Drack, M.; Schwödiauer, R.; Graz, I.; Bauer-Gogonea, S.; Bauer, S.; Someya, T. *Nature* **2013**, *499*, 458–463.
- (19) Krebs, F.; Tromholt, T.; Jørgensen, M. *Nanoscale* **2010**, *2*, 873–886.
- (20) Lipomi, D. J.; Bao, Z. *Energy Environ. Sci.* **2011**, *4*, 3314.
- (21) Martinez, R. V.; Branch, J. L.; Fish, C. R.; Jin, L.; Shepherd, R. F.; Nunes, R. M. D.; Suo, Z.; Whitesides, G. M. *Adv. Mater.* **2013**, *25*, 205–212.
- (22) Suo, Z.; Ma, E.; Gleskova, H.; Wagner, S. *Appl. Phys. Lett.* **1999**, *74*, 1177.
- (23) Tahk, D.; Lee, H. H.; Khang, D.-Y. *Macromolecules* **2009**, *42*, 7079.
- (24) Lipomi, D. J.; Chong, H.; Vosgueritchian, M.; Mei, J.; Bao, Z. *Sol. Energy Mater. Sol. Cells* **2012**, *107*, 355–365.
- (25) Chen, Z.; Lee, M. J.; Shahid Ashraf, R.; Gu, Y.; Albert-Seifried, S.; Meedom Nielsen, M.; Schroeder, B.; Anthopoulos, T. D.; Heeney, M.; McCulloch, I.; Sirringhaus, H. *Adv. Mater.* **2012**, *24*, 647–652.
- (26) Dou, L.; You, J.; Hong, Z.; Xu, Z.; Li, G.; Street, R. A.; Yang, Y. *Adv. Mater.* **2013**, *25*, 6642–6671.
- (27) McCulloch, I.; Heeney, M.; Bailey, C.; Genevicius, K.; Macdonald, I.; Shkunov, M.; Sparrowe, D.; Tierney, S.; Wagner, R.; Zhang, W.; Chabinyc, M. L.; Kline, R. J.; McGehee, M. D.; Toney, M. F. *Nat. Mater.* **2006**, *5*, 328–333.
- (28) Li, G.; Zhu, R.; Yang, Y. *Nat. Photon.* **2012**, *6*, 153–161.
- (29) Hösel, M.; Søndergaard, R. R.; Jørgensen, M.; Krebs, F. C. *Energy Technol.* **2013**, *1*, 102–107.
- (30) Facchetti, A. *Chem. Mater.* **2011**, *23*, 733–758.
- (31) Liao, S.-H.; Li, Y.-L.; Jen, T.-H.; Cheng, Y.-S.; Chen, S.-A. *J. Am. Chem. Soc.* **2012**, *134*, 14271.
- (32) Osedach, T. P.; Andrew, T. L.; Bulović, V. *Energy Environ. Sci.* **2013**, *6*, 711.
- (33) Anctil, A.; Babbitt, C. W.; Raffaelle, R. P.; Landi, B. J. *Prog. Photovolt Res. Appl.* **2013**, *21*, 1541–1554.
- (34) Scherf, U.; Gutacker, A.; Koenen, N. *Acc. Chem. Res.* **2008**, *41*, 1086–1097.
- (35) Printz, A. D.; Savagatrup, S.; Burke, D. J.; Purdy, T. N.; Lipomi, D. J. *RSC Adv.* DOI: 10.1039/C4RA00029C.
- (36) Pearson, A. J.; Wang, T.; Dunbar, A. D. F.; Yi, H.; Watters, D. C.; Coles, D. M.; Staniec, P. a.; Iraqi, A.; Jones, R. a. L.; Lidzey, D. G. *Adv. Funct. Mater.* **2013**, *24*, 659–667.
- (37) Spano, F. C. *J. Chem. Phys.* **2005**, *122*, 234701.
- (38) Ren, G.; Wu, P.; Jenekhe, S. A. *Chem. Mater.* **2010**, *22*, 3300–3306.
- (39) Wu, P.-T.; Ren, G.; Jenekhe, S. A. *Macromolecules* **2010**, *43*, 3306–3313.
- (40) Stafford, C. M.; Harrison, C.; Beers, K. L.; Karim, A.; Amis, E. J.; VanLandingham, M. R.; Kim, H.-C.; Volksen, W.; Miller, R. D.; Simonyi, E. E. *Nat. Mater.* **2004**, *3*, 545–550.
- (41) Bowden, N.; Brittain, S.; Evans, A. G.; Hutchinson, J. W.; Whitesides, G. M. *Nature* **1998**, *393*, 146.
- (42) Bowden, N.; Huck, W. T. S.; Paul, K. E.; Whitesides, G. M. *Appl. Phys. Lett.* **1999**, *75*, 2557.
- (43) VanLandingham, M. R.; Villarrubia, J. S.; Guthrie, W. F.; Meyers, G. F. *Macromol. Symp.* **2001**, *167*, 15–43.
- (44) Seitz, J. *J. Appl. Polym. Sci.* **1993**, *49*, 1331–1351.
- (45) Vosgueritchian, M.; Lipomi, D. J.; Bao, Z. *Adv. Funct. Mater.* **2012**, *22*, 421–428.
- (46) Du Pasquier, A.; Miller, S.; Chhowalla, M. *Sol. Energy Mater. Sol. Cells* **2006**, *90*, 1828–1839.
- (47) Chiechi, R. C.; Weiss, E. A.; Dickey, M. D.; Whitesides, G. M. *Angew. Chem., Int. Ed.* **2008**, *47*, 142–144.
- (48) Dickey, M. D.; Chiechi, R. C.; Larsen, R. J.; Weiss, E. A.; Weitz, D. A.; Whitesides, G. M. *Adv. Funct. Mater.* **2008**, *18*, 1097–1104.
- (49) Palleau, E.; Reece, S.; Desai, S. C.; Smith, M. E.; Dickey, M. D. *Adv. Mater.* **2013**, *25*, 1589–1592.
- (50) Clark, J.; Chang, J.-F.; Spano, F. C.; Friend, R. H.; Silva, C. *Appl. Phys. Lett.* **2009**, *94*, 163306.
- (51) Clark, J.; Silva, C.; Friend, R.; Spano, F. *Phys. Rev. Lett.* **2007**, *98*, 206406.
- (52) Spano, F. C.; Clark, J.; Silva, C.; Friend, R. H. *J. Chem. Phys.* **2009**, *130*, 074904.
- (53) Turner, S. T.; Pingel, P.; Steyrleuthner, R.; Crossland, E. J. W.; Ludwigs, S.; Neher, D. *Adv. Funct. Mater.* **2011**, *21*, 4640–4652.
- (54) Turro, N. J. *Modern Molecular Photochemistry*; 1st ed.; University Science Books: Sausalito, CA, 1991.
- (55) Louarn, G.; Trznadel, M. *J. Phys. Chem.* **1996**, *3654*, 12532–12539.
- (56) Nielsen, L. E.; Landel, R. F. *Mechanical Properties of Polymers and Composites*, Rev. and Expanded ed.; CRC Press: Boca Raton, FL, 1993.
- (57) McCullough, R. D. *Adv. Mater.* **1998**, *10*, 93–116.
- (58) Bruner, C.; Dauskardt, R. *Macromolecules* **2014**, DOI: 10.1021/ma402215j.
- (59) Verswyvel, M.; Monnaie, F.; Koeckelberghs, G. *Macromolecules* **2011**, *44*, 9489–9498.
- (60) Ge, J.; He, M.; Qiu, F.; Yang, Y. *Macromolecules* **2010**, *43*, 6422–6428.
- (61) Ge, J.; He, M.; Yang, X.; Ye, Z.; Liu, X.; Qiu, F. *J. Mater. Chem.* **2012**, *22*, 19213–19221.
- (62) He, M.; Zhao, L.; Wang, J.; Han, W.; Yang, Y.; Qiu, F.; Lin, Z. *ACS Nano* **2010**, *4*, 3241–3247.
- (63) Nandan, B.; Kandpal, L. D.; Mathur, G. N. *J. Appl. Polym. Sci.* **2003**, *90*, 2887.
- (64) Ramiro, J.; Equizazabal, J. I.; Nazabal, J. *Polym. Adv. Technol.* **2003**, *14*, 129–136.
- (65) Chen, T.; Wu, X.; Rieke, R. *J. Am. Chem. Soc.* **1995**, *117*, 233–244.
- (66) Koch, F. P. V.; Heeney, M.; Smith, P. *J. Am. Chem. Soc.* **2013**, *135*, 13699–13709.
- (67) Pal, S.; Nandi, A. K. *Macromolecules* **2003**, *36*, 8426–8432.
- (68) Plate, N. A.; Shibaev, V. P. *P. J. Polym. Sci., Macromol. Rev.* **1974**, *8*, 117–253.
- (69) Reimschuessel, H. K. *J. Polym. Sci., Polym. Chem. Ed.* **1979**, *17*, 2447–2457.
- (70) Chen, S.; Ni, J.-M. *Macromolecules* **1992**, *25*, 6081.
- (71) Kim, J. Y.; Frisbie, C. D. *J. Phys. Chem. C* **2008**, *112*, 17726–17736.
- (72) Treat, N.; Mates, T.; Hawker, C. *Macromolecules* **2013**, *46*, 1002–1007.
- (73) Koppe, M.; Scharber, M.; Brabec, C.; Duffy, W.; Heeney, M.; McCulloch, I. *Adv. Funct. Mater.* **2007**, *17*, 1371–1376.

- (74) Kline, R. J.; McGehee, M. D.; Kadnikova, E. N.; Liu, J.; Frechet, J. M. J.; Toney, M. F. *Macromolecules* **2005**, *38*, 3312–3319.
- (75) Brinkmann, M.; Wittmann, J.-C. *Adv. Mater.* **2006**, *18*, 860–863.
- (76) Wu, P.-T.; Xin, H.; Kim, F. S.; Ren, G.; Jenekhe, S. A. *Macromolecules* **2009**, *42*, 8817–8826.
- (77) Pingel, P.; Zen, A. *Adv. Funct. Mater.* **2010**, *20*, 2286–2295.
- (78) Roehling, J. D.; Batenburg, K. J.; Swain, F. B.; Moulé, A. J.; Arslan, I. *Adv. Funct. Mater.* **2013**, *23*, 2115–2122.
- (79) Liu, F.; Gu, Y.; Shen, X.; Ferdous, S.; Wang, H.-W.; Russell, T. P. *Prog. Polym. Sci.* **2013**, *38*, 1990–2052.
- (80) Brady, M. A.; Su, G. M.; Chabinyc, M. L. *Soft Matter* **2011**, *7*, 11065.